Drowning incidents and conditions due to hidden flash rips in Lake Michigan

Yuli Liu [1,2] and Chin H. Wu[2*]

[1]School of Marine Sciences, Nanjing University of Information Science and Technology, Nanjing, China
[2]Department of Civil and Environmental Engineering, University of Wisconsin-Madison, Madison, WI, USA

Abstract

Flash rips are episodic bursts of water jetting offshore, which can lead to drowning incidents by sweeping swimmers offshore without warning, thus posing a hidden and unrecognized danger to beachgoers. This study reveals hazards of flash rips by investigating a series of drowning incidents along coasts of Lake Michigan during a series of storm events on July 18-21, 2019. Occurrences and causes of flash rips were depicted through webcam image observations, storm features of atmospheric disturbances, hydrodynamic circumstances of wind waves and meteorologically induced water level fluctuations, and model-reconstructed nearshore circulations. Results shows that flash rips were generated during or after storms through nearshore processes of storm-induced wind waves and meteorologically induced water level fluctuations. With small wind waves, low water level fluctuations, and a timing delay of rip occurrences relative to the causative convective storms, flash rips pose a hidden hazard to unaware swimmers. Historical observations for incidents in Lake Michigan between 2002 and 2019 further show that dry conditions or fair weathers and a calm water signature at the beach can likely generate unexpected hidden flash rips, resulting in the highest drowning risks. There is an urgent need for communication, education, and prediction/forecast of hidden flash rips to the Laurentian Great Lakes and worldwide coastal communities.

Keywords: drowning, flash rips, convective storms, meteorologically induced water level fluctuations, Lake Michigan

*Correspondence to Chin H. Wu, Email: chinwu@engr.wisc.edu

1. Introduction

Drowning can pose threats to global coastal communities. Numbers of worldwide drownings are estimated to be 320,000 annual deaths, ranking the 3rd among the leading causes of unintentional injury-related deaths based upon the World Health Organization (WHO, 2014). In the Laurentian Great Lakes, nearly 1029 drownings were reported by the Great Lakes Surf Rescue Project over the past 12 years (GLSRP, 2021). Moreover, the per capita number of drownings in the Great Lakes Region with a population of approximately 34 million is comparable to drowning rates in oceanic coastal regions throughout the United States and in countries like Australia and Costa Rica (Vlodarchyk et al., 2019). Many drownings are attributed to rip currents (Brewster et al., 2019; Brighton et al., 2013), strong seaward water flows that are hazardous to people regardless of their swimming abilities (Castelle et al., 2016; Gensini & Ashley, 2010). In the United States, approximately 150 deaths per year are caused by rip currents (Lushine, 1991; Brewster et al., 2019). According to the Great Lake Current Incident Database (GLCID, 2021), a total of 223 fatalities and 480 rescues during 2002-2020 on the United States and Canadian coasts of the Great Lakes were attributed to rip currents and wind waves (Gensini & Ashley, 2010; Meadows et al., 2011; Vlodarchyk et al., 2019). Rip currents can appear at barred beaches as bathymetry-controlled rips, near headlands and coastal structures as boundary-controlled rips, at beaches connected to rivers or estuaries as outlet currents, and even at featureless beaches as flash rips, which are transient, episodic, and nonstationary rip currents (Shepard et al. 1941; Castelle et al., 2016; Gallop et al., 2020; Dalrymple et al., 2011). Swimmers can suddenly get swept by a flash flow towards offshore deep water, where panic and exhaustion usually lead to drownings (MacMahan et al., 2006; Brander et al., 2011). While rip current hazards have been communicated and taught to beachgoers and beach managers, the hidden danger of flash rips has not yet been widely recognized (Linares et al., 2019).

Flash rips are generated through various nearshore processes (Castelle et al., 2016). First, shear instabilities of longshore currents, under highly oblique incidence waves (Feddersen, 2014), can generate transient vortices as non-fixed flows toward offshore (Özkan-Haller & Kirby, 1999). Second, short-crested wave breaking creates along-crest variations in wave dissipation (Kirby & Derakhti, 2019; Peregrine, 1998) to create vorticities (Castelle et al., 2016; Clark et al., 2012). A fraction of those short-scale vorticities that are not dissipated by bottom friction can cascade into larger-scale surf zone eddies as offshore-directed water jets (Feddersen, 2014; Spydell & Feddersen, 2009). Third, wave groups and infra-gravity waves (Long & Özkan-Haller, 2009; MacMahan et al., 2004) can generate alongshore variations of radiation stress gradients that are imbalanced by spatial pressure gradients. The induced wave set-ups of high temporal variability (Johnson & Pattiaratchi, 2004) can result in pulsating flows as transient rip currents (Dalrymple, 1975; Uchiyama et al., 2017). Fourth, rapid runups and drawdowns of water levels, different from energetic wind waves, can induce flash rips by generating unsteady vortices that are shed to the offshore (Linares et al., 2019). Specifically, meteorologically induced high frequency water level fluctuations like meteotsunamis and seiches are commonly seen in the Laurentian Great Lakes (Anderson & Mann, 2021; Bechle et al., 2015, 2016; Linares et al., 2016). Seiches are basin-scale standing waves in an enclosed or semi-enclosed water body (Rabinovich, 2009). Meteotsunamis are sub-basin scale propagating waves with periods from a few minutes to two hours (Monserrat et al., 2006). Under certain hydrodynamic circumstances, all above mentioned processes can generate hidden flash rips that are undetected by beach users.

Convective storms can be associated with hidden danger of flash rips (Linares et al., 2019).

Structures of convective storms in the Laurentian Great Lakes can be generally classified into four types: complex, linear, bow, and cluster (Bechle et al., 2015; Fowle & Roebber, 2003; Gallus et al., 2008; Workoff et al., 2012). Complex and linear storms feature large (>500 km^2), long-lived (>3 hours), organized structures (Fowle & Roebber, 2003; Workoff et al., 2012) that create sustained wind stresses and pressure perturbations (Bechle et al., 2015, 2016). Bow storms such as "derechos" (Johns & Hirt, 2019) occur less frequently but are responsible for most severe winds (Changnon & Kunkel, 2006) and several well-defined pressure anomaly events (Šepić & Rabinovich, 2014; Wertman et al., 2014). Cluster storms, in contrast, consist of small (<40 km^2), unorganized, and separated areas (Workoff et al., 2012; Weisman & Klemp, 1986). Convective storms are found to generate more than 100 meteotsunamis per year in the Great Lakes, which have been overlooked (Bechle et al., 2016). Linares et al., 2019 found that 16% of rip current incidents in Lake Michigan during 2002-2017 were reported on the same days when convective storm-induced meteotsunamis were detected. Furthermore, a recent study by Liu & Wu, (2019) observed 90% of flash rips co-occurred with convective storms over a two-year period (2016-2017) on the west coast of Lake Michigan. Nevertheless, it remains unclear what features of convective storms and hydrodynamic (water-level fluctuation and wind wave) circumstances can generate flash rips.

The objective of this paper is to depict what conditions lead to elevated drowning risks due to flash rips that usually go undetected by beachgoers. In this study, occurrences of flash rips were identified by processed webcam images. Observations were used to characterize features of convective storms that might lead to drowning incidents. In addition, observed hydrodynamic circumstances of meteorologically induced water level fluctuations and wind waves were used to describe plausible pathways and processes to generate flash rips. Integrated atmospheric-hydrodynamic modeling was employed to reveal causes of flash rips by reconstructing detailed nearshore circulations at incident locations. An approximately 20-year dataset of historical flash rip incidents and associated hydrodynamic circumstances and features of storms in Lake Michigan were compiled and characterized. This paper, for the first time, highlights that many drowning incidents in Lake Michigan are related to a lack of beachgoer awareness regarding hidden flash rips. Three conditions that could lead to development of flash rips are discovered. These conditions with elevated risks are crucial to be delivered to coastal communities.

2. Materials and methods

2.1. Study site and event description

Lake Michigan, with a coastal population above 2 million, has been identified as one of the hotspots for rip current-related drownings (Gensini & Ashley, 2010; Vlodarchyk et al., 2019). According to the Great Lakes Current Incident Database (GLCID, 2021), more than 70% of drowning incidents in five Laurentian Great Lakes occurred on coasts of Lake Michigan. The lake with an averaged depth of 85 m spans approximately 500 km in the latitudinal and 100 km in the longitudinal directions (Fig. 1). Wind wave climate in Lake Michigan is dominated by locally generated, fetch-limited waves with short periods and broadly distributed directions, like the other Laurentian Great Lakes (Meadows et al., 2011; Rao & Schwab, 2007). These characteristics of wind waves are quite different from those that generate rip currents in the ocean environment (Castelle et al., 2016). Recent studies revealed that propagating meteotsunamis occur about 50 times per year in Lake Michigan (Bechle et al., 2016) and are primarily forced by convective storms (Bechle et al., 2015). Specifically, in southern Lake Michigan, meteotsunamis are likely generated by Proudman resonance (Proudman, 1929) with storms of speeds close to 30 m/s

(Bechle et al., 2015). In the region of northern Lake Michigan with shelf slopes of 0.007-0.0012 (Linares et al., 2016), meteotsunamis are possibly formed by Greenspan resonance (Greenspan, 1956) through trapped edge wave speeds greater than 14 m/s (As-Salek & Schwab, 2004, Linares et al., 2018). Estimated periods of seiches reported by As-Salek & Schwab (2004) are 9.0, 5.2, 3.7, 3.1, 2.5 and 2.2 hours in longitudinal direction and 2.1 and 1.3 hours in the transverse direction in Lake Michigan. In short, convective storms over Lake Michigan are prone to cause wind waves and high frequency water level fluctuations (e.g., meteotsunamis, and seiches), which are all possible hydrodynamic drivers to the occurrence of flash rips.

In this study, an example event of multiple drowning incidents, which occurred consecutively during a four-day period from July 18 to 21, 2019 along coasts of Lake Michigan (Fig. 1), was examined. The first drowning fatality occurred around 0000 UTC of July 19 on the east coast near Ludington (Ramirez, 2019). The second incident occurred a few hours later around 1630-1700 UTC on the southeast shore near South Haven where three men were rescued (GLCID, 2021). The third drowning fatality occurred around 2300 UTC on the southwest shore near Kenosha (GLSRP, 2021). The next day, a strong "derecho" landed on the northwest shore at 0225 UTC of July 20. Damages were reported around 0630-1045 UTC on the northeast shore near Little Traverse Bay (Zucker, 2019) and the north shore near Manistique (Borden, 2019), similar to the previously reported meteotsunami events in Lake Michigan (Bechle et al., 2015, Anderson & Mann 2021). Afterwards, the fourth drowning fatality occurred on the south shore near Michigan City around 0130 UTC of July 21 (GLCID, 2021). Later, on the same day, the fifth incident on the east coast at Ludington around 1600-1900 UTC when a man trapped by a river outlet current was rescued (GLCID, 2021) and the sixth incident occurred on the southeast coast at Chicago occurred around 2030 UTC ended with one drowning fatality and one rescue (GLSRP, 2021). In short, in the 6 incidents that occurred within 4 days, at least 4 fatalities and 5 rescues were reported at 5 nearshore locations in Lake Michigan. Some incidents (I2, I4, I5) were identified to be current-related according to the GLCID, while others are yet to be further examined. With convective storms crossing Lake Michigan and high-frequency water level fluctuations reported, the nearshore hydrodynamics at different incident locations exhibited different characteristics, from large waves at Ludington (I1) to calm waters at Kenosha (I3), according to local newspaper reports (Fig 1). With the information, it is thus hypothesized that the drowning incidents might be related to flash rips.

2.2. Image, storm, and hydrodynamic observations

Images of beach webcams on Lake Michigan were examined to identify occurrences of flash rips on days of drowning incidents. A webcam installed at the North Beach of Port Washington, WI (Liu & Wu, 2019), captured images during the study period. Images from other webcam sources including the Great Lakes Meteorological Real-Time Coastal Observation Network, and the EarthCam network for public webcams around Lake Michigan were also reviewed, however no additional footage outside of Port Washington was available for the study. Flash rips were identified based upon sediment plume signatures on recorded images at 5-second intervals. Procedures of image processing consist of image segmentation, ortho- rectification, and plume detection (Bechle et al. 2012, Liu & Wu, 2019; Wanek and Wu, 2006). Timings of flash rip occurrences were characterized. Durations of flash rips were counted from the first appearance of sediment plumes until no offshore-directed propagations for the same plume were detected. Multiple flash rips that appeared intermittently with time intervals of less than 1 hour were consolidated to be a single occurrence.

Storm features of atmospheric pressure and wind disturbances in Lake Michigan were characterized. NEXRAD radar reflectivity composite images from the Iowa Environmental Mesonet with 1-km spatial resolution and 5-min intervals were used to identify storm structures. The timing for convective storms crossing Lake Michigan was determined as starting when reflectivity areas with values >25dBZ initially crossed the shoreline and ending when the reflectivity areas completely left the entire lake perimeter. A widely used storm classification criteria (Bechle et al., 2015) was used to define storm structures as convective types, such as complex, cluster, linear and bow; and not convective types, such as frontal or cyclonic systems. Storm disturbances were depicted based on 1-min data of atmospheric pressures, surface wind speeds and wind directions from the 16 Automated Surface Observing System (ASOS) around Lake Michigan (see Fig. 1). A high-pass digital filter with 2-hour cut-off frequency was used to obtain storm-related high-frequency atmospheric pressure fluctuations. The isochronal analysis method (Šepić et al., 2009) was used to determine storm propagation speeds and directions. The temporal gradients of pressure perturbations and wind shear stresses at maximum speeds (Bechle et al., 2016; Linares et al., 2018) were used to calculate relative contributions of atmospheric pressure (P) and wind (W) disturbances to initiate wind waves and water level fluctuations.

Hydrodynamic circumstances related to the storms in Lake Michigan were characterized by following procedures. First, water level data in 6-min intervals were obtained from 10 observation stations operated by NOAA National Ocean Service (see Fig. 1). Second, a high-pass digital filter with a 6-hour cut-off frequency (Bechle et al., 2015) was applied on the water level time series to obtain oscillations in the meteotsunami wave frequency band (Monserrat et al, 2006).

The zero-crossing method (Sorensen, 2006) was employed to calculate wave heights and periods of individual waves from the filtered time series. Third, a meteotsunami-identification criterion (Linares et al., 2016) were applied to identify meteotsunamis such that: the (long) wave height exceeded gauge-specific thresholds (Bechle et al., 2016) and the period fell in the 2-min to 2-hour high-frequency range. We categorized fluctuating water level changes (ΔWL, height from crest to trough of the water level time series) into low ($\Delta WL < 0.1m$), modest ($0.1 < \Delta WL < 0.3m$), and high ($\Delta WL > 0.3m$) circumstances. Lastly, wind wave data from 15 available water buoys in Lake Michigan (see Fig. 1) operated by the NOAA National Data Buoy Center (NDBC) were compiled. Wave statistics including significant wave height (H_S), mean wave direction (*MWD*) and peak wave period (T_p) were reported in 30-min or 1-hour intervals, depending on data availability. In this study, wave heights H_S smaller than 0.3 m, between 0.3 m and 0.6 m, and larger than 0.9 m were categorized as small, moderate, and large wave circumstances respectively.

2.3. Integrated atmospheric-hydrodynamic modeling

Integrated atmospheric-hydrodynamic modeling was implemented to simulate nearshore conditions of the incident locations. The Semi-implicit Cross-scale Hydroscience Integrated System Model (SCHISM), developed by Zhang & Baptista (2008) and Zhang et al. (2016), was coupled with the 3rd generation spectral Wind Wave Model (WWM III), developed by Roland et al. (2012), through wave-current interactions (Yu & Slinn, 2003; Hass et al., 2003). This type of coupled model has been successfully employed to simulate rip currents caused by longshore shear currents (Özkan-Haller & Kirby, 1999), wave group-generated rip vortices (Long & Özkan-Haller, 2009), and meteotsunami-generated dangerous rips (Linares et al., 2019). In the SCHISM-WWM

III implementation, current velocities and water levels are solved in the unsteady three-dimensional Reynolds-averaged Navier–Stokes equation under the hydrostatic approximation with the k-ε turbulence scheme (Umlauf & Burchard, 2003), wind and bottom shear stresses based upon the quadratic formulation (Ardhuin et al., 2010; Bechle et al., 2014; Janssen, 1991), and wave radiation stress gradients (Longuet-Higgins & Stewart, 1964) through the wave action balance equation in the WWM III. Meanwhile, wave fields are updated based on the evolving current velocities and water elevations from the SCHISM. In this study, the two models were simultaneously run with a time interval of $\Delta t = 5$ sec and the coupling was set at every time step. Both short time interval and coupling set-up at every time step are critical for simulating wave-induced vortices and flash rips (Castelle et al., 2016; Linares et al., 2019). Atmospheric pressure and wind disturbances of the convective storms for 10 days including before, during, and after the 4-day July 18-21, 2019 storm were reconstructed for the purpose of modeling inputs in the following steps. First, ambient atmospheric pressure and wind data were at an hourly interval extracted from the output of the NOAA High-Resolution Rapid Refresh (HRRR) atmospheric model with a spatial resolution of 3 km (Benjamin et al., 2016). Second, storm disturbances were constructed as trapezoidal shaped perturbations with a uniform bandwidth (Bechle et al., 2014; Linares et al., 2016, 2018). The trapezoid parameters were estimated based on the time series of observed atmospheric pressures and wind speeds at storm passed ASOS stations with a 1-min interval. Third, the HRRR ambient atmospheric features and the high-frequency storm disturbances were assimilated to match with all ASOS stations across the Lake Michigan. The atmospheric input has a time resolution of 1 min and spatial resolution of 3 km which ensures high-frequency storm features can be faithfully represented. This reconstruction of atmospheric disturbances has been shown to faithfully simulate wind waves and meteorologically induced water level fluctuations (Linares et al., 2019).

Multi-scale domain discretization with varying sizes of mesh was employed to the whole lake. Fig.2 shows a total of 1,125,678 triangular unstructured elements with coarse resolutions of 5 km in the mid-lake and finer resolution of 50-100 m along the entire nearshore region. To delineate detailed shorelines and coastal slopes for modeling meteotsunami transformations (Bechle & Wu, 2014), nearshore bathymetry with a horizontal resolution of 100 m was interpolated from the high-spatial resolution LiDAR data of the 2012 USACE NCMP Topography Survey (Office for Coastal Management, 2014). On the nearshore scale, near the five incident locations (Kenosha, WI, Chicago, IL Michigan City, IN, Ludington, and MI; South Haven, see Fig. 2 c-g respectively), we further refined mesh resolutions to 2 m at shorelines and gradually increased to 100 m toward offshore where the nearshore scale mesh is seamlessly merged into the large lake scale mesh. At Port Washington where observations were made, nearshore meshes of similar resolutions (Fig. 2b) were constructed to validate model results. As illustrated by Linares et al. (2019) and Huang et al. (2021), use of the high model mesh resolution at nearshore areas is critical to resolve circulations or rip currents due to interactions of water level fluctuations and wind waves.

3. Results

3.1. Flash rip occurrences

Observed occurrences of flash rips in Lake Michigan during the four-day period of the six drowning incidents on July 18-22, 2019 (Fig. 1) and a series of convective storms, are described. A total of 11 flash rip occurrences, denoted chronologically as R1 to R11 (see color rectangles in Fig. 3a, b), are identified based on image evidence of rip-induced sediment plumes captured by a nearshore camera at Port Washington, WI. At the same time, a total of six convective structures, denoted chronologically as S1 to S6, are also shown in snapshots of radar reflectivity images in Fig 4 (a-f), respectively. Characteristics of observed flash rips exhibit intermittent and episodic features, as the numbers of flash rips in each occurrence were found to be irregular and discontinuous, represented by different colors of the rectangles in Fig. 3 (a, b). Transient flash rips with observed durations between 25 to 245 sec and intervals of less than an hour, are consistent with previously reported flash rip observations (Floc'h et al., 2018; Liu & Wu, 2019; Murray et al., 2013). Timings of flash rip occurrences relative to the convective storms (shaded blue rectangles) and the drowning incidents (yellow dots) are registered on the time series plots of Fig 3 (a,b). For example, both R1 and R4 flash rips in Fig. 3c and Fig. 3d appeared after the storm (S1) and (S2) with delays of 1 hour and 5 hours, respectively. Flash rip R7 (Fig. 3e) occurred during the beginning of the storm (S4), while R10 flash rip (Fig. 3f) was found during the later hours of the storm (S5). No occurrence of flash rips was identified during or after the storm (S6). Particularly, flash rips such as R4 (Fig 3d) and R10 (Fig. 3f) occurred when the weather appeared to be at a dry condition and the nearshore water surface looked calm.

Hydrodynamic circumstances for flash rips are further examined based on observed wind wave heights (H_S) at the nearby NDBC buoy (45013, see Fig. 1) and water level fluctuations ($\Delta\eta$ = displacement relative to mean water level and ΔWL = height from crest to trough of $\Delta\eta$) at the nearby NOS water level gauge (MKE, see Fig. 1). As shown in Fig 3 (a,b), both R1 and R7 flash rips (Fig. 3c, e) occurred under a moderate H_S and high ΔWL condition; R4 flash rip (Fig. 3d) appeared under a small H_S and low ΔWL condition; and flash rip R10 (Fig. 3f) was under a small H_S but high ΔWL condition. For all the 11 occurrences observed, approximately

87% of flash rips occurred when H_S were below 0.9 m, i.e., small and moderate wave circumstances (Fig. 3a). Approximately 74% of flash rips exhibited when ΔWL between 0.1 m and 0.30 m, i.e., low to modest water level fluctuations (Fig. 3b). Overall, flash rips observed at Port Washington during and after storms were under the circumstances of small to moderate wind waves and low and modest water level fluctuations, which may explain unawareness of hazardous flash rips to beachgoers.

3.2. Storm features of atmospheric pressure and wind disturbances

Features (i.e., structure, magnitude, and duration) of atmospheric pressure and wind disturbances associated with the six convective storm structures from July 18 to 21 are chronologically depicted in Fig. 5 a-d. The first storm (S1, see Fig. 4a) was a convective complex that propagated southeasterly at 14.6 m/s. Fig. 5a shows a pressure drop with a rate of 1.4 hPa/10min and wind increase to the maximum speed of 15.4 m/s with a direction change along the storm propagation at the KMKG, the ASOS station at Muskegon on the east side of Lake Michigan (see Fig. 1). At the farther southeastern KBIV (see Fig. 1), a steep pressure plunged with a rate of 2.3 hPa/10min but the increase of wind occurred approximately 20 minutes later. The second storm was a convective cluster (see S2, Fig. 4b) that propagated eastwards at 22.8 m/s. Fig. 5b shows that storm disturbances of a pressure gradient of 1.9 hPa/10min and a wind speed of 12.3 m/s initially appeared on the west coast at the KMKE (see Fig.1). After arriving on the east coast at the KMKG, the storm became weaker with a pressure gradient of 1.0 hPa/10min and wind speeds under 10 m/s. This feature is consistent with the previous finding that atmospheric perturbations of clusters usually become weaker after crossing the lake (Workoff et al., 2012). The third and fourth storms, reported as “derechos” of July 2019

(Erdman, 2019), were a convective bow (S3, Fig. 4c) propagating southward at 16.5 m/s and a linear convection (S4, Fig. 4d) moving at 20.7 m/s toward the southeast, respectively. Fig. 5c shows a train of pressure perturbations with a pressure jump of 3.7 hPa/10 min during S3 and two pressure jumps of 6.2 hPa/10min and 6.9 hPa /10min during S4 at the KGRB on the northwestern coast (see Fig. 1). These pressure disturbances were comparable to or even greater than the magnitude of 2-5 hPa/10 min in largest meteotsunami events worldwide (Šepić & Rabinovich, 2014). Corresponding maximum speeds were 15.9 m/s and 18.0 m/s in S3 and S4, respectively. The fifth and sixth storms were a convective cluster (S5, Fig. 4e) and a convective complex (S6, Fig. 4f) that propagated eastward at 9.8 m/s and 7.0 m/s, respectively. These two storms had relatively small pressure gradients (less than 1 hPa/10min) and wind speeds (less than 8 m/s), as shown in Fig. 5d. In short, not only large visible storms like S1, S3 and S4 occurred during the 4-day incident event, but also less noticeable smaller storms like S2, S5, and S6 passed through portions of Lake Michigan.

The six convective storms with associated atmospheric pressure (P) or wind (W) disturbances to initiate water level fluctuations like meteotsunamis and wind waves are summarized in Table 1. Among the six storms, two (S2 and S6) were wind-dominated ($W>60\%$), one (S5) was pressure-dominated ($P>60\%$), and the other three (S1, S3 and S4) had equal contributions of wind and pressure ($40\%\leq W\leq 60\%$ and $40\%\leq P\leq 60\%$). Storms with equal contributions of wind and pressure disturbances such as S1, S3, and during S4 storms result in larger wave heights to initiate more than 6 flash rips in R1, R5, and R7 occurrences, respectively, (Fig. 3a, b). In comparison, after storms with either a dominated wind or pressure disturbance such as S2 and S5, flash rips occurred under small or moderate wave heights (R2, R3, R4, R10, and R11), which can be a hidden danger to unaware beachgoers.

3.3. Hydrodynamic circumstances of water level fluctuations and wind waves

Meteorologically induced water level fluctuations leading to flash rips through three possible pathways are described. One possibility is meteotsunami-induced edge waves that generate longshore currents (Anderson et al., 2015; Bechle & Wu, 2014; Ewing et al., 1954). In Fig. 5e, meteotsunamis (green box) occurred at the Calumet Harbor, the NOS water level gage located on the southwest corner of the lake (CAL in Fig. 1). Meanwhile, near the incident I1 at Ludington, MI, small water level fluctuations with a period of 55 min at the LUD (Fig. 1) propagated like edge waves along the coast. Similarly, Fig. 5f shows that after the meteotsunami event at the CAL, the edge wave propagated northward. Small water level fluctuations with a period of 35 min were observed at Milwaukee (MKE in Fig. 1), near where the incident I3 happened. The calculated time for the propagating edge wave speed (Greenspan, 1956) along the southwest coast between Port Washington and Kenosha is 218 min, close to 223 min inferred from the time between observed R4 occurrence of flash rips and the incident I3 in Fig. 3 a and b. The matching between the calculated time and observation time suggests that meteotsunami-induced edge waves may induce strong longshore currents that resulted in flash rips at multiple locations. The second possibility is meteotsunami-induced water level drawdowns, which have been shown to generate unexpected rip currents and caused several drownings in Lake Michigan (Linares et al., 2019). In Fig. 5g, the incident I4 (Fig. 1) at Michigan City occurred during fast-receding water levels after a large meteotsunami event at CAL. Superposition of the two smaller meteotsunami-induced edge waves from the east coast (LUD) and the west coast (MKE) swiftly converged to a larger wave at the south shore, similar to the conditions in a severe 1954 meteotsunami event (Bechle et al., 2014) and in a 2018 atmospheric gravity wave-induced meteotsunami event (Anderson & Mann, 2021), to generate strong return currents or flash rips near the incident location. The third possibility is meteotsunami-induced seiches. Before the incident I5 (see Fig. 5h), the meteotsunamis occurred during UTC0330-1130 at LUD and during UTC0330-UTC1500 at CAL. Water levels at LUD continued to fluctuate from UTC1600 to UTC1830 with a period of 50 min like the situation at MKE. The time lag between LUD and MKE is 25-min, half of the oscillation period, suggesting that the observed meteorologically induced water level fluctuations could be standing seiches (Linares et al., 2018). Unforeseen seiches were previously suggested to generate rip currents in Lake Michigan (Meadows et al., 2011). In short, meteotsunami-induced longshore currents, drawdowns, and seiches are three possible pathways that led to unexpected flash rips. Particularly, meteotsunami waves initiated from storms somewhere else would propagate through the three pathways to the drowning incident locations without notice, thus posing a hidden danger to swimmers.

Wind waves to generate flash rips at incident locations through two possible nearshore processes are described. One possibility is shear instability of longshore currents generated under oblique incident waves (Özkan-Haller & Kirby, 1999). Fig. 5i shows that at UTC2355 oblique incident waves from southwest were approaching toward the east coast near Ludington where the incident (I1) happed. The statement is based on wave data obtained from the NDBC buoy 45024 (see Fig. 1), with significant wave height (H_S) of 1.28 m, a peak wave period (Tp) of 5.5 sec, and a mean wave direction (*MWD*, relative to the True North) of 247° (Table 1). Similarly, near Michigan City during the incident I4 (Fig. 5k) and near Chicago during I6 (Fig. 5l), observed oblique incident waves with moderate to large wave heights (H_S = 0.75 ~ 0.93 m, Table 1) could possibly induce flash rips. The second possibility is breaking-induced vorticities (Kirby & Derakhti, 2019; Long & Özkan-Haller, 2009; MacMahan et al., 2004) caused by shore-normal incidence waves. In Fig. 5j, at the time of the incident I2, moderate wind waves with H_S = 0.6 m were approaching from west with MWD of 280° towards South Haven on the east coast. The shore-normal incidence waves can create breaking-induced vortices to cause episodic offshore-directed flash rips (Dalrymple, 1975; Uchiyama et al., 2017). Overall, energetic oblique wind waves or moderate shore-normal incidence waves through two nearshore processes possibly led to hazardous flash rips near the incident locations.

3.4. Reconstruction of flash rips at incident locations

Flash rips near drowning incident locations that are reconstructed by the integrated atmospheric-hydrodynamic modeling are illustrated in the following four incident cases. At 0000 UTC on July 19, water level fluctuations $\Delta\eta$ of amplitudes less than 0.05 m (Fig. 6a) are negligible to generate currents near Ludington of the incident I1 (Fig. 6b). Instead, large wind waves with a significant wave height of H_S ~ 1.3 m due to the southeastern winds (Fig. 5a, i) obliquely approach toward Ludington (Fig. 6c). Driven by wave-induced strong meandering shear currents, pairs of negative (blue) and positive (red) vortices with the magnitude of 0.1 s^{-1} are induced on the nearshore region (see the zoom-in view in Fig. 6d). The vorticities are 15 ~ 30 meters apart, consistent to the length scale of previously observed flash rips (Liu & Wu, 2019). Four identified flash rip jets are numbered. Spacings of the generated rips are between 50 ~ 100 m with offshore distances up to 100 m in rip ②, similar to those commonly observed on the nearshore areas in Lake Michigan (Liu & Wu, 2019) and the ocean (Murray et al., 2013; Suanda & Feddersen, 2015). Several flash rip jets with the speed higher than 1.0 m/s are hazardous and can be a possible cause of the drowning tragedy near Ludington. Similar results for incident I6 near Chicago, not shown here for brevity, are also found.

At 1640 UTC on July 19, modest water level fluctuations with $\Delta\eta$ ~ 0.10 m (Fig. 6e) are meteotsunami-generated propagating edge waves, yielding the northward longshore currents near South Haven in incident I2 (Fig. 6f). Small to moderate waves with H_S ~ 0.6 m caused by the southeastern winds (see Fig. 5b, j) are developed (Fig. 6g). In the zoom-in nearshore region, several sporadic small flash rips (see ②-④ in Fig. 6h) with vorticity values of ~0.05 s^{-1} are generated through the circulation cell due to interactions of edge wave induced longshore currents and southeastern wind waves. A pronounced rip jet ① with a speed of 0.5 m/s is created from a vortex pair shedding offshore, similar to the process that the meteotsunami-generated flash rips reported in a previous study (Linares et al., 2019). The jet spatially extends to 100 m from the shoreline, comparable to those in Case I (Fig. 6d). Differently, the sporadic rip jets in Case II caused by unnoticeable water level fluctuations and small to moderate wind waves, could catch swimmers off guard. Flash rips could be the cause of incident I2. Similar results at 2300 UTC on the southwest shore near Kenosha for the drowning tragedy of incident I3 at Kenosha, not shown here for brevity, are also found.

At 0130 UTC of July 21, receding water levels or drawdowns with $\Delta\eta$ > 0.15 m on the south shore in Fig. 6i are created by the reflection of the two converged meteotsunami-induced edge waves from the east and west coasts, similar to the condition in the 1954 event (Behcle & Wu, 2014). As a result, seaward cross-shore currents, i.e., reflected outward currents, are generated near Michigan City where incident I4 occurred (Fig. 6i, j). The outflow destabilizes persisting inward longshore currents, creating a meandering behavior (Fig. 6j). Moderate waves with H_S ~ 0.7 m caused by the rapidly changing winds (Fig. 5c, k) are developed (Fig. 6k). In the zoom-in nearshore region (Fig. 6l), three flash rip jets are driven by vorticity pairs of magnitudes larger than 0.1 s^{-1} and lengths of 30-50 meters. Offshore velocities in rip ① are larger than 1.0 m/s, same as those in Fig. 5d. Rip spacings are up to 150 m between rip ②-③ and the offshore distances extend beyond 100 meters from the shoreline, larger than those in Fig. 5d. The combined effects of meteotsunami drawdown-induced offshore currents and wave-induced nearshore currents can amplify the spatial scales of flash rips, resulting in swimmers being trapped by the high-speed outward flows, as a possible cause of incident I4 near Michigan City.

At 1630 UTC on July 21, seiches induced by meteotsunamis are exhibited by the spatial distribution of water level fluctuations (Fig. 6m). Near Ludington where the incident I5 occurred, southward longshore currents are generated near the nodal points, i.e., $\Delta\eta \sim 0$ (Fig. 6n). Small wind waves with H_S ~0.45 m caused by the northern winds (Fig. 5d) are developed (Fig. 6o). In the zoom-in nearshore region (Fig. 6p), six flash rip jets are identified in the 300-m nearshore span, more than those in Fig 6(d). Flash rips ①, ② and ③ are seiche-induced meandering shear currents, which are destabilized under the incident waves and turn into the offshore-directed rip flows. Closer to the shoreline, flash rip ④, ⑤ and ⑥ are generated through vorticity pairs with the magnitude of 0.05 s^{-1}. Under the relatively low $\Delta\eta$ and small H_S, the offshore extent of rip ① and ② are less than 100 m. Nevertheless, the maximum velocities of rip jets reach to 0.5 m/s, comparable to the rip velocities under relatively high $\Delta\eta$ in the edge wave-generated rip (Fig. 6h). Unforeseen flash rips caused by instability of longshore shear currents in meteotsunami-induced seiches are revealed for the first time, which supports the conjecture of seiche-induced rip currents in Lake Michigan (Meadows et al., 2011). The flash rips under the hydrodynamic circumstances of small wind waves and low water level fluctuations were likely not noticed by beachgoers, which likely elevated the drowning risk at the beach near incident I5 (Fig. 1). The water level fluctuations could amplify nearshore currents (Linares et al.,

2018) and modulate outlet currents. The compound drowning risk, due to outlet currents and meteorologically induced water level fluctuations, is suggested for future studies.

4. Discussion

4.1. Hydrodynamic circumstances near drowning incident locations

Hydrodynamic circumstances of flash rips and incidents between 2002 and 2019 in Lake Michigan reported by the Great Lake Current Incident Database (GLCID, 2021) are compiled and plotted. The nearly 20-year dataset provides all hydrodynamic circumstances in addition to those observed during the event of July 18-22, 2019 in Lake Michigan. Given that no direct flash rip observations for the incidents were available, flash rips were extracted from a total of 186 records by excluding bathymetry-controlled rip currents that occurred in channels, boundary-controlled rip currents near structures (Castelle et al., 2016), and those at river outlets identified by GLCID (National Weather Service, 2019). The most-likely flash rips related incidents had a total of 185 individual victims. For each flash rip incident, hydrodynamic circumstances of water level changes (ΔWL) and significant wave heights (H_S) are compiled from historical data of the NOS gauges and NDBC buoys. For those with no nearby available nearshore wave data, the H_s of nearshore wave heights at the incident locations are estimated from offshore wave buoy data using the wave shoaling equation (Sorensen, 2006). The estimations were verified by comparing the estimated wave heights against the measured waves in the 30 events with available nearshore wave data, yielding an averaged difference of 10% (or an absolute difference of 0.09 m). Fig. 7 shows the distribution of flash rip incidents versus H_S and ΔWL. The majority 65% of the incidents (117 victims) occurred under the circumstance with $H_S < 1$ m and $\Delta WL < 0.3$ m, i.e. the "small H_S – low ΔWL" quadrant. The remaining 35% of incidents were in other quadrants: 25% in the "large H_S — low ΔWL" quadrant, 9% in the "small H_S — high ΔWL" quadrant, and 1% in the "large H_S — high ΔWL" quadrant. Among the 10 incidents that yielded more than four victims in one single incident, 6 were flash rips in the small H_S — low ΔWL quadrant. Of importance, more victims and incidents occurred in hidden flash rips under the hydrodynamic circumstances with small wind waves and low meteorologically induced water level fluctuations, which may not be easily detected by beachgoers.

4.2. Storm features related to flash rip incidences

Storm features related to flash rips are characterized in the following four aspects. First, the seasonality of storms in Laurentian Great Lakes overlaps with the peak season of beachgoers (Bechle et al., 2015, 2016), prompting coastal populations to be more vulnerable to flash rip hazards. Large complex and linear convective storms, most common during late-spring to mid-summer (Bechle et al., 2016), can cause large wind waves and high water level fluctuations, resulting in hazardous flash rips such as I1 and I4. Second, radar reflectivity maps from the NEXRAD composite image database show that annually 50% of convective storm events tend to occur consecutively in 3 days or more. Consecutive small cluster storms like the events described in Fig. 4 as S2 and S5 tend to result in more hidden flash rips than expected. Third, fast-moving convective storms (Bechle et al., 2015; 2016), in comparison with not convective storms (Anderson & Mann, 2021; Shi et al., 2020) like frontal, cyclonic systems, and atmospheric gravity waves seem to be associated with most of the flash-rip induced incidents (see yellow and orange dots in Fig. 7). The dots associated with convective-storm incidents tend to cluster in the left quadrants, suggesting that hardly noticeable water level changes like meteotsunamis, in comparison to visible wind waves, are more likely to cause drowning incidents (see Cases 2, 3, and 4 in Section 3.4). This statement is consistent with the recent finding that meteotsunami-induced rips are not sporadic but more frequently related to drowning incidents (Linares et al., 2019). In comparison, only 25% of incidents were associated with not convective storms (see blue dots in Fig. 7) and most occurred with noticeably large wave height H_S. Lastly, the timing of storms is found to occur up to 1-2 days before the flash rip incidents, which counts for almost 50% of all convective-associated incidents (see yellow dots in Fig. 7). After storm disturbances have already passed the lake, the initiated water level fluctuations (e.g., meteotsunamis) would continuously propagate like edge waves or be rebounded as standing seiches. These meteorologically induced water level fluctuations could be transformed through the three possible pathways described in Section 3.3 to generate hidden flash rips at locations under a dry condition or a fair weather, i.e., far from the initial storm event. Two examples are storms S3 and S5 that led to incidents I3 and I5 (Table 1). Timing delay of flash rips relative to convective storms can disguise the danger from swimmers (or beachgoers). In short, storm features including (i) seasonality of storms overlapping with the swimming season, (ii) more small consecutive cluster storms generating more hidden flash rips than expected, (iii) convective storm induced meteorological water level fluctuations (not visible wind waves) highly correlated to drowning incidents, and (iv) the time delay of visible storms relative to flash rip occurrences can further expose beachgoers to flash rips.

4.3 Conditions of high-risk hidden flash rips

Hidden flash rips pose a high drowning risk to beachgoers. Dry conditions or fair weathers, light winds (Castelle et al., 2019; Houser et al., 2019), small wind waves, or undetectable water level changes (Fallon et al., 2018), conditions suggested by the observation in Fig. 7, can deceive beachgoers into entering the water at a time when the drowning risk is elevated (Ferrari et al., 2020; Linares et al., 2019). Three conditions of high-risk hidden flash rips are encapsulated in Fig. 8, based on the event of July 18-21, 2019, and the drowning incidents of 2002-2019 in Lake Michigan. The first condition (Fig. 8a) occurs on a day of fair weather with a series of small convective cluster storms. At the beach, small or moderate waves with mild breakings on the nearshore result in hidden flash rips, like those flash rips observed at Port Washington (see Fig. 3). The second condition (Fig. 8b) occurs when a convective storm passes across the lake but far away from the beach. The weather at the beach is at a dry condition and the nearshore water appears relatively calm without wind waves breaking. The meteotsunami-generated edge waves initiated elsewhere propagate to the beach hours later to create hidden flash rips, similar to those happened to I2 at South Haven and I3 at Kenosha. The third condition (Fig. 8c) occurs after a convective storm passes across the lake. At the beach, the weather returns to have a dry condition and the nearshore water appears tranquil. Nevertheless, the unnoticeable reflected meteotsunami waves suddenly appear to generate hidden flash rips, similar to those that happened during I4 at Michigan City. In short, the three conditions featured with a pleasant dry condition or a fair weather and a calm water surface signature at the beach can attract bathers to enter the nearshore water with unexpected hidden flash rips, resulting in the highest drowning risks. Specifically, the false perception of safety by beachgoers to unseen danger of hidden flash rips have not yet been noticed and reported before on the Great Lakes, as far as the authors are aware.

5. Conclusions

Hidden flash rips were revealed to relate to a series of drowning incidents on the coasts of Lake Michigan during a series of storm events on July 18-22, 2019. Observed flash rips occurred during or after convective storms with features of atmospheric pressure and wind disturbances. Hydrodynamic circumstances of meteorologically induced water level fluctuations and wind waves generated flash rips near the drowning incident locations through processes of energetic wind waves, meteotsunami-induced longshore currents, water level drawdowns, and seiche-induced currents. Flash rip incidents in Lake Michigan in 2002-2019 shows that many drowning incidents occur under small waves and water level fluctuations, a hidden circumstance which can hardly be detected by beachgoers. Drowning risks are further elevated by features of storms including the seasonality of storms overlapping with the swimming season, small consecutive cluster storms generating hidden flash rips, and the time delay of visible storms relative to flash rip occurrences. In short, three conditions, featured with dry conditions or fair weathers and a calm water signature at the beach, can attract bathers to enter the nearshore water with unexpected hidden flash rips, resulting in the highest drowning risks. Findings of this study reveal that many past drowning incidents in Lake Michigan are related to hidden conditions due to flash rips, which have not been well recognized before. There is an urgent need for communication, education, and prediction/forecast of hidden flash rips to the Laurentian Great Lakes and worldwide coastal communities.

Acknowledgements

This work was supported in part by the NOAA Coastal Storms Program, University of Wisconsin Sea Grant Institute (UW-Sea Grant), and Wisconsin Coastal Management Program. We specifically thank Dr. Alvaro Linares for guiding the mutiple-scale integrated atmospheric-hydrodynamic modeling and providing insights to clarify meteotsunamis-induced hazadous flash rips. Dr. Adam Bechle for his valuable comments and suggestion on interpreting the data is recognized. In addition, Ms Marie Zhuikov at UW-Sea Grant and Ms Mary Possin at Dept. of Civil and Environmental Engineering at UW-Madison are acknowledged for their helpful editorial comments. Ms. Moira Harrington at UW-Sea Grant for her dedication to communicating rip current hazards to the Great Lakes community are accredited. Last but not least, insightful comments and valuable suggestions provided by three anonymous reviewers and editors are highly appreciated.

References

Anderson, E.J., Bechle, A.J., Wu, C.H., Schwab, D.J., Mann, G.E., Lombardy, K.A., 2015. Reconstruction of a meteotsunami in Lake Erie on 27 May 2012: Roles of atmospheric conditions on hydrodynamic response in enclosed basins. J. Geophys. Res. Ocean. 120, 8020–8038. https://doi.org/10.1002/2015JC010883

Anderson, E.J., Mann, G.E., 2021. A high-amplitude atmospheric inertia–gravity wave-induced meteotsunami in Lake Michigan. Nat. Hazards, 106, 1489–1501. https://doi.org/10.1007/s11069-020-04195-2

Ardhuin, F., Rogers, E., Babanin, A. V., Filipot, J.F., Magne, R., Roland, A., van der Westhuysen, A., Queffeulou, P., Lefevre, J.M., Aouf, L., Collard, F., 2010. Semiempirical dissipation source functions for ocean waves. Part I: Definition, calibration, and validation. J. Phys. Oceanogr. 40, 1917–1941. https://doi.org/10.1175/2010JPO4324.1

As-Salek, J.A., Schwab, D.J., 2004. High-Frequency Water Level Fluctuations in Lake Michigan. J. Waterw. Port, Coastal, Ocean Eng. 130, 45–53. https://doi.org/10.1061/(ASCE)0733-950X(2004)130:1(45)

Benjamin, S.G., Weygandt, S.S., Brown, J.M., Hu, M., Alexander, C.R., Smirnova, T.G., Olson, J.B., James, E.P., Dowell, D.C., Grell, G.A., Lin, H., Peckham, S.E., Smith, T.L., Moninger, W.R., Kenyon, J.S., Manikin, G.S., 2016. A North American hourly assimilation and model forecast cycle: The rapid refresh. Mon. Weather Rev. 144, 1669–1694. https://doi.org/10.1175/MWR-D-15-0242.1

Bechle, A.J., Wu, C.H., Liu, W.C., Kimura, N.. 2012. Development and application of an automated river-estuary discharge imaging system. J. Hydraulic Eng., 138, 327-339. https://doi.org/10.1061/(ASCE)HY.1943-7900.0000521

Bechle, A.J., Wu, C.H., Kristovich, D.A.R., Anderson, E.J., Schwab, D.J., Rabinovich, A.B., 2016. Meteotsunamis in the Laurentian Great Lakes. Sci. Rep. 6, 37832. https://doi.org/10.1038/srep37832

Bechle, A.J., Kristovich, D.A.R., Wu, C.H., 2015. Meteotsunami occurrences and causes in Lake Michigan. J. Geophys. Res. Ocean. 120, 8422–8438. https://doi.org/10.1002/2015JC011317

Bechle, A.J., Wu, C.H., 2014. The Lake Michigan meteotsunamis of 1954 revisited. Nat. Hazards 74, 155–177. https://doi.org/10.1007/s11069-014-1193-5

Borden, E. (2019, July 23). Manistique feeling effects of high water levels. *UpperMichigansSource.com.*https://www.uppermichiganssource.com/content/news/Manistique-feeling-effects-of-storm-surge--513063971.html

Brander, R.W., Bradstreet, A., Sherker, S., MacMahan, J., 2011. Responses of Swimmers Caught in Rip Currents: Perspectives on Mitigating the Global Rip Current Hazard. Int. J. Aquat. Res. Educ. 5. https://doi.org/10.25035/ijare.05.04.11

Brewster, B.C., Gould, R.E., Brander, R.W., 2019. Estimations of rip current rescues and drowning in the United States. Nat. Hazards Earth Syst. Sci., 19, 389-39. https://doi.org/10.5194/nhess-19-389-2019

Brighton, B., Sherker, S., Brander, R., Thompson, M., Bradstreet, A., 2013. Rip current related drowning deaths and rescues in Australia 2004-2011. https://doi.org/10.5194/nhess-13-1069-2013

Castelle, B., Scott, T., Brander, R. McCarroll, J. 2016. Rip current types, circulation and hazard. Earth-Sci. Rev. 163 1–21. https://doi.org/10.1016/j.earscirev.2016.09.008

Castelle, B., Scott, T., Brander, R., McCarroll, J., Robinet, A., Tellier, E., de Korte, E., Simonnet, B., Salmi, L.-R., 2019. Environmental controls on surf zone injuries on high-energy beaches. Nat. Hazards Earth Syst. Sci. 19, 2183–2205. https://doi.org/10.5194/nhess-19-2183-2019

Clark, D.B., Elgar, S., Raubenheimer, B., 2012. Vorticity generation by short-crested wave breaking. Geophys. Res. Lett. 39, 24604. https://doi.org/10.1029/2012GL054034

Dalrymple, R.A., 1975. A mechanism for rip current generation on an open coast. J. Geophys. Res. 80, 3485–3487. https://doi.org/10.1029/JC080i024p03485

Dalrymple, R.A., MacMahan, J.H., Reniers, A.J.H.M., Nelko, V., 2011. Rip Currents. Annu. Rev. Fluid Mech. 43, 551–581. https://doi.org/10.1146/annurev-fluid-122109-160733

Davis, W.M., 1925. The undertow myth. Science 61, 206–208

Erdman, J., 2019. A Derecho, a Widespread Destructive Thunderstorm Wind Event, Swept Across Minnesota, Wisconsin and Michigan. The Weather Channel.

Ewing, M., Press, F., Donn, W.L., 1954. An Explanation of the Lake Michigan Wave of 26 June 1954. Science 120, 684–6. https://doi.org/10.1126/science.120.3122.684

Fallon, K.M., Lai, Q., Leatherman, S.P., 2018. Beachgoer's recognition of rip current hazard at Miami Beach, Florida. Ocean Coast. Manag. 165, 63–70. https://doi.org/https://doi.org/10.1016/j.ocecoaman.2018.08.011

Feddersen, F., 2014. The Generation of Surfzone Eddies in a Strong Alongshore Current. J. Phys. Oceanogr. 44, 600–617. https://doi.org/10.1175/JPO-D-13-051.1

Ferrari, M., Carpi, L., Pepe, G., Mucerino, L., Schiaffino, C.F., Brignone, M., Cevasco, A., 2019. A geomorphological and hydrodynamic approach for beach safety and sea bathing risk estimation. Sci. Total Environ. 671, 1214–1226. https://doi.org/10.1016/j.scitotenv.2019.03.378

Floc'h, F., Mabiala, G.R., Almar, R., Castelle, B., Hall, N., Du Penhoat, Y., Scott, T., Delacourt, C., 2018. Flash Rip Statistics from Video Images. J. Coast. Res. 81, 100–106. https://doi.org/10.2112/SI81-013.1

Fowle, M.A., Roebber, P.J., 2003. Short-Range (0–48 h) Numerical Prediction of Convective Occurrence, Mode, and Location. Weather Forecast. 18, 782–794. https://doi.org/10.1175/1520-0434(2003)018<0782:SHNPOC>2.0.CO;2

Gallam, C. (2019, July 23). Man pulled from Lake Michigan near Washington Park Beach dies. *WSBT 22*. https://wsbt.com/news/local/update-man-pulled-from-lake-michigan-near-washington-park-beach-passes-away

Gallop, S.L., Kennedy, D.M.,Loureiro, C. Naylor, L.A., Muñoz-Pérez, J.J., Jackson, D.W.T., Fellowes, T.E.2020. Geologically controlled sandy beaches: Their geomorphology morphodynamics and classification. Science of the Total Environment. 731, 139123. https://doi.org/10.1016/j.scitotenv.2020.139123

Gallus, W.A., Snook, N.A., Johnson, E. V., 2008. Spring and Summer Severe Weather Reports over the Midwest as a Function of Convective Mode: A Preliminary Study. Weather Forecast. 23, 101–113. https://doi.org/10.1175/2007WAF2006120.1

Gensini, V.A., Ashley, W.S., 2010. An examination of rip current fatalities in the United States. Nat. Hazards 54, 159–175. https://doi.org/10.1007/s11069-009-9458-0

Great Lakes Current Incident Database, 2021. In: Great Lakes Current Incidents and Statistics. https://www.weather.gov/greatlakes/beachhazards_stats

Great Lakes Surf Rescue Project, 2021. Statistics. http://www.glsrp.org/statistics/ Accessed Date: December 30, 2021.

Greenspan, H.P., 1956. The generation of edge waves by moving pressure distributions. https://doi.org/10.1017/S002211205600038X

Haas, K.A., Svendsen, I.A., Haller, M.C., Zhao, Q., 2003. Quasi-three-dimensional modeling of rip current systems 108, 10–1. https://doi.org/10.1029/2002jc001355

Houser, C., Lehner, J., Cherry, N., Wernette, P., 2019. Machine learning analysis of lifeguard flag decisions and recorded rescues. Nat. Hazards Earth Syst. Sci. 19, 2541–2549. https://doi.org/10.5194/nhess-19-2541-2019

Huang, C., Anderson, E.J., Liu, Y., Ma, G., Mann, G., Xue., P. 2021. Evaluating essential processes and forecast requirements for meteotsunami-induced coastal flooding. Nat. Hazards. https://doi.org/10.1007/s11069-021-05007-x

Janssen, P., 1991. Quasi-linear theory of wind-wave generation applied to wave forecasting. J. Phys. Oceanogr. 21, 1631–1642. https://doi.org/10.1175/1520-0485(1991)021<1631:QLTOWW>2.0.CO;2

Johnson, D., Pattiaratchi, C., 2004. Transient rip currents and nearshore circulation on a swell-dominated beach. J. Geophys. Res. 109, C02026. https://doi.org/10.1029/2003JC001798

Kirby, J.T., Derakhti, M., 2019. Short-crested wave breaking. Eur. J. Mech. - B/Fluids 73, 100–111. https://doi.org/10.1016/J.EUROMECHFLU.2017.11.001

Linares, Á., Wu, C.H., Anderson, E.J., Chu, P.Y., 2018. Role of Meteorologically Induced Water Level Oscillations on Bottom Shear Stress in Freshwater Estuaries in the Great Lakes. J. Geophys. Res. Ocean. 123, 4970–4987. https://doi.org/10.1029/2017JC013741

Linares, Á., Bechle, A.J., Wu, C.H., 2016. Characterization and assessment of the meteotsunami hazard in northern Lake Michigan. J. Geophys. Res. Ocean. 121, 7141–7158. https://doi.org/10.1002/2016JC011979

Linares, Á., Wu, C.H., Bechle, A.J., Anderson, E.J., Kristovich, D.A.R., 2019. Unexpected rip currents induced by a meteotsunami. Sci. Rep. 9, 2105. https://doi.org/10.1038/s41598-019-38716-2

Liu, Y., Wu, C.H., 2019. Lifeguarding Operational Camera Kiosk System (LOCKS) for flash rip warning: Development and application. Coast. Eng. 152, 103537. https://doi.org/10.1016/j.coastaleng.2019.103537

Long, J.W., Özkan-Haller, H.T., 2009. Low-frequency characteristics of wave group–forced vortices. J. Geophys. Res. 114, C08004.

Longuet-Higgins, M.S., 1970. Longshore currents generated by obliquely incident sea waves: 1. J. Geophys. Res. 75, 6778–6789. https://doi.org/10.1029/JC075i033p06778

Lushine, J.B., 1991. A Study of Rip Current Drownings and Related Weather Factors. Natl. Wea. Dig. 16, 13-19.

MacMahan, J.H., Reniers, A.J.H.M., Thornton, E.B., Stanton, T.P., 2004. Infragravity rip current pulsations. J. Geophys. Res. C Ocean. 109. https://doi.org/10.1029/2003jc002068

MacMahan, J.H., Thornton, E.B., Reniers, A.J.H.M., 2006. Rip current review. Coast. Eng. 53, 191–208.

Meadows, G., Purcell, H., Guenther, D., Meadows, L., Kinnunen, R.E., Clark, G., 2011. Rip Currents in the Great Lakes: An Unfortunate Truth, in: Leatherman, S., Fletemeyer, J. (Eds.), Rip Currents: Beach Safety, Physical Oceanography, and Wave Modeling. CRC Press, pp. 199–214.

Monserrat, S., Vilibić, I., Rabinovich, A.B., 2006. Meteotsunamis: atmospherically induced destructive ocean waves in the tsunami frequency band. Nat. Hazards Earth Syst. Sci. 6, 1035–1051. https://doi.org/10.5194/nhess-6-1035-2006

Murray, T., Cartwright, N., Tomlinson, R., 2013. Video-imaging of transient rip currents on the Gold Coast open beaches. J. Coast. Res. 165, 1809–1814. https://doi.org/10.2112/SI65-306.1

National Weather Service, 2021. Beach Hazards Incident Statistics.

https://www.weather.gov/greatlakes/beachhazards_stats

Office for Coastal Management, 2014. Coastal Topobathy Lidar. https://www.coast.noaa.gov/digitalcoast/data/jalbtcx.html. Accessed date: December 9, 2019

Özkan-Haller, H.T., Kirby, J.T., 1999. Nonlinear evolution of shear instabilities of the longshore current: A comparison of observations and computations. J. Geophys. Res. Ocean. 104, 25953–25984. https://doi.org/10.1029/1999JC900104

Peregrine, D.H., 1998. Surf Zone Currents. Theor. Comput. Fluid Dyn. 10, 295–309. https://doi.org/10.1007/s001620050065

Police: Man dies in apparent drowning in Kenosha. (2019, July19). *FOX 6 Now Milwaukee*. https://www.fox6now.com/news/police-man-dies-in-apparent-drowning-in-kenosha

Police ID man who died after being rescued from Lake Michigan. (2019, July 21). *NBC Chicago.* https://www.nbcchicago.com/news/local/police-identify-lake-michigan-drowning-victim-saturday/78405/

Proudman, J., 1929. The Effects on the Sea of Changes in Atmospheric Pressure. Geophys. J. Int. 2, 197–209. https://doi.org/10.1111/j.1365-246X.1929.tb05408.x

Rabinovich, A.B., 2009. Seiches and Harbor Oscillations, in: Handbook of Coastal and Ocean Engineering. WORLD SCIENTIFIC, pp. 193–236. https://doi.org/10.1142/9789812819307_0009

Rao, Y.R., Schwab, D.J., 2007. Transport and Mixing Between the Coastal and Offshore Waters in the Great Lakes: a Review. J. Great Lakes Res. 33, 202–218. https://doi.org/https://doi.org/10.3394/0380-1330(2007)33[202:TAMBTC]2.0.CO;2

Ramirez,C. (2019, July 19). Ludington girl, 14, dies after drowning in Lake Michigan. *The*

Detroit News. https://www.detroitnews.com/story/news/local/michigan/2019/07/19/ludington-girl-14-dies-after-drowning-lake-michigan/1776063001/

Roland, A., Zhang, Y.J., Wang, H. V., Meng, Y., Teng, Y.C., Maderich, V., Brovchenko, I., Dutour-Sikiric, M., Zanke, U., 2012. A fully coupled 3D wave-current interaction model on unstructured grids. J. Geophys. Res. Ocean. 117. https://doi.org/10.1029/2012JC007952

Šepić, J., Rabinovich, A.B., 2014. Meteotsunami in the Great Lakes and on the Atlantic coast of the United States generated by the “derecho” of June 29–30, 2012. Nat. Hazards 74, 75–107. https://doi.org/10.1007/s11069-014-1310-5

Šepić, J., Vilibić, I., Belušić, D., 2009. Source of the 2007 Ist meteotsunami (Adriatic Sea). J. Geophys. Res. 114, C03016. https://doi.org/10.1029/2008JC005092

Šepić, J., Vilibić, I., Strelec Mahović, N., 2012. Northern Adriatic meteorological tsunamis: Observations, link to the atmosphere, and predictability. J. Geophys. Res. Ocean. 117. https://doi.org/10.1029/2011JC007608

Shepard, F.P., Emery, K.O., Lafond, E.C., 1941. Rip Currents: A process of geological importance. Journal of Geology, 49, 338-369. https://doi.org/10.1086/624971

Shi, L., Olabarrieta, M., Nolan, D.S., Warner, J.C., 2020. Tropical cyclone rainbands can trigger meteotsunamis. Nat. Commun. 11, 1–14. https://doi.org/10.1038/s41467-020-14423-9

Sorensen, R.M. 2006, Basic Coastal Engineering, Third Edition, Springer, New York. ISBN: 978-0-387-23333-8

Spydell, M., Feddersen, F., 2009. Lagrangian Drifter Dispersion in the Surf Zone: Directionally Spread, Normally Incident Waves. J. Phys. Oceanogr. 39, 809–830. https://doi.org/10.1175/2008JPO3892.1

Suanda, S.H., Feddersen, F., 2015. A self-similar scaling for cross-shelf exchange driven by transient rip currents. Geophys. Res. Lett. 42, 5427–5434. https://doi.org/10.1002/2015GL063944

Uchiyama, Y., McWilliams, J.C., Akan, C., 2017. Three-dimensional transient rip currents: Bathymetric excitation of low-frequency intrinsic variability. J. Geophys. Res. Ocean. 122, 5826–5849. https://doi.org/10.1002/2017JC013005

Umlauf, L., Burchard, H., 2003. A generic length-scale equation for geophysical turbulence models. J. Mar. Res. 61, 235–265. https://doi.org/10.1357/002224003322005087

Vlodarchyk, B., Olivito, A., Houser, C., 2019. Spatial and Temporal Variation of Surf Drownings in the Great Lakes: 2010–17. J. Coast. Res. 35, 794. https://doi.org/10.2112/JCOASTRES-D-18-00027.1

Wertman, C.A., Yablonsky, R.M., Shen, Y., Merrill, J., Kincaid, C.R., Pockalny, R.A., 2014. Mesoscale convective system surface pressure anomalies responsible for meteotsunamis along the U.S. East Coast on June 13th, 2013. Sci. Rep. 4. https://doi.org/10.1038/srep07143

Workoff, T.E., Kristovich, D.A.R., Laird, N.F., LaPlante, R., Leins, D., 2012. Influence of the Lake Erie Overlake Boundary Layer on Deep Convective Storm Evolution. Weather Forecast. 27, 1279–1289. https://doi.org/10.1175/WAF-D-11-00076.1

World Health Organization, 2014. Global report on drowning: preventing a leading killer. World Health Organization.

Wanek, J.M. and Wu, C.H. 2006. Automated trinocular stereo imaging system for three-dimensional surface wave measurements. Ocean Engineering. 33, 723-747. https://doi.org/10.1016/J.OCEANENG.2005.05.006

Yu, J., Slinn, D.N., 2003. Effects of wave-current interaction on rip currents. J. Geophys. Res. C

Ocean. 108, 33–1. https://doi.org/10.1029/2001jc001105

Zhang, Y.J., Ye, F., Stanev, E. V., Grashorn, S., 2016. Seamless cross-scale modeling with SCHISM. Ocean Model. 102, 64–81. https://doi.org/10.1016/J.OCEMOD.2016.05.002

Zhang, Y., Baptista, A.M., 2008. SELFE: A semi-implicit Eulerian–Lagrangian finite-element model for cross-scale ocean circulation. Ocean Model. 21, 71–96. https://doi.org/10.1016/J.OCEMOD.2007.11.005

Zucker, S. (2019, July 22). Rapid water rise causes shoreline damage early Saturday. *News-Review*. https://www.petoskeynews.com/story/news/local/2019/07/22/rapid-water-rise-causes-shoreline-damage-early-saturday/44221983/

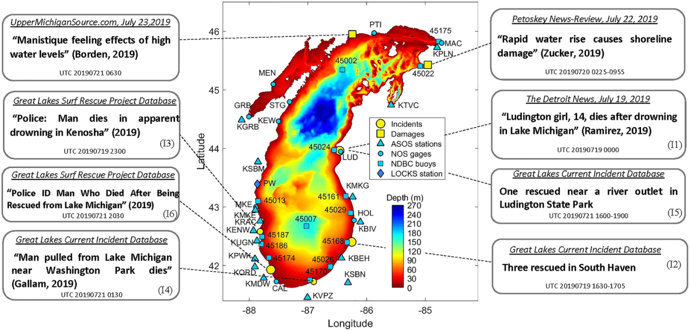

Fig. 1. Study site of Lake Michigan with bathymetry depicted in the colormap. Six drowning incidents (yellow dots) occurred in a 4-day period of July 18-21, 2019. The incidents and related water level-damages (yellow squares), reported by the Great Lakes Current Incident Database (GLCID), Great Lakes Surf Rescue project (GLSRP) Database, or online newspaper, are shown. Available observations for atmospheric and hydrodynamic conditions include 16 Automated Surface Observation System (ASOS) meteorology stations, 10 water level gauges operated by the National Ocean Service (NOS), 15 wave buoys operated by the National Data Buoy Center (NDBC), and 1 webcam at Port Washington (PW).

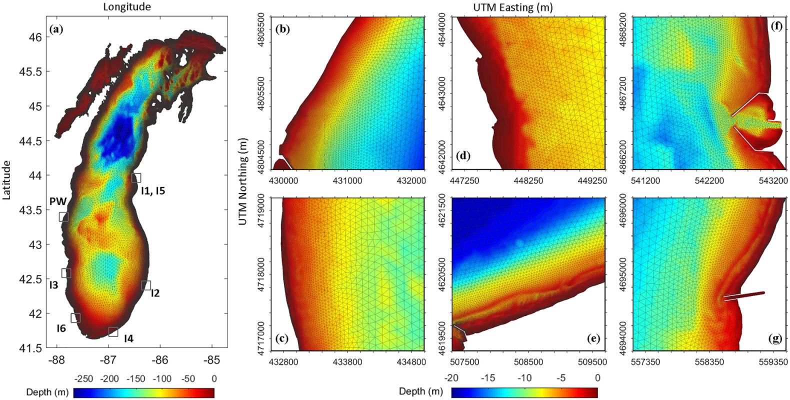

Fig. 2 Unstructured meshes of the integrated atmospheric-hydrodynamic model: (a) Lake Michigan, with grey boxes indicating refined nearshore regions including (b) Port Washington (PW) where flash rip image observations were available and the five locations where drowning incidents were reported during July 18-21, 2019: (c) Kenosha (I3), (d) Chicago (I6), (e) Michigan City (I4), (f) Ludington (I1, I5), and (g) South Haven (I2).

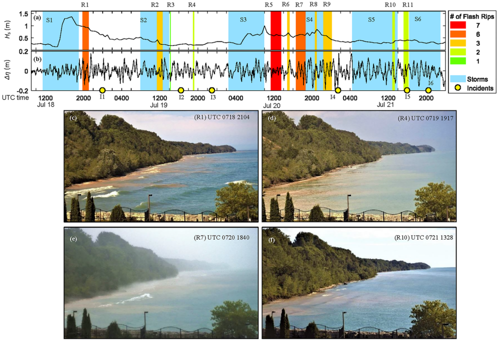

Fig. 3: A total of eleven flash rip occurrences at Port Washington, WI and the six convective storms in colored rectangles plotted on the time series of: (a) significant waves heights (H_s) at the NDBC buoy 45013, and (b) water level oscillations ($\Delta\eta$) at the NOS gage MKE. The number (#) of flash rips in each occurrence is represented by colors in the legend box. The six reported incidents are shown in yellow solid dots. Images of flash rips were captured at (c) UTC2104 of July 18, (d) UTC1917 of July 19, (e) UTC 1840 of July 20, and (f) UTC 1328 of July 21 by the real-time nearshore camera of the Lifeguarding Operational Camera Kiosk System (LOCKS).

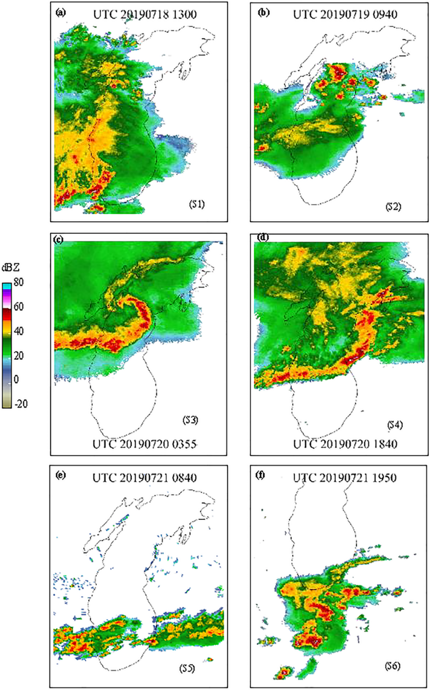

Fig. 4: Snapshots of radar reflectivity images of the six convective storm structures.

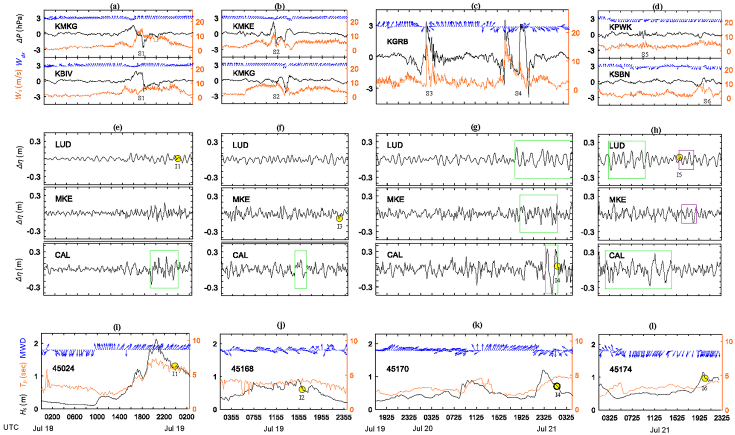

Fig. 5: Time series of the convective storm event of July 18-21, 2019 for: (a-d) atmospheric pressure fluctuations (ΔP), surface wind speeds (W_s) and directions (W_{dir}) observed at ASOS stations; (e-h) water level fluctuations ($\Delta\eta$) observed at NOS water level gauges, with meteotsunamis identified in green boxes and seiches in purple boxes; (i-l) significant wave height (H_s), peak wave period (T_p) and mean wave direction (MWD) observed at NDBC wave buoys. Timing of the reported incidents are labeled as yellow solid dots at the nearest NOS or NDBC stations in (e-l).

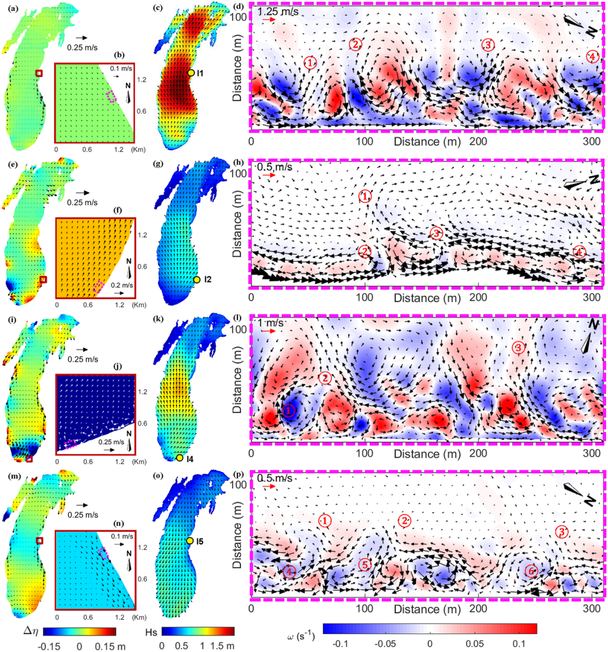

Fig 6. Snapshots of model-reconstructed flash rips at locations of incidents, I1 in (a-d), I2 in (e-h), I4 in (i-l), and at the beach near I5 in (m-p). (a,e,i,m) are current velocity fields in arrows plotted on water level fluctuations ($\Delta\eta$) colormaps for whole Lake Michigan with zoom-in views (red box) in (b,f,j,n); (c,g,k,o) are wind wave directions in arrows plotted on significant wave height (H_s) colormaps for whole Lake Michigan, with incident locations shown in yellow circles; and (d,h,l,p) are zoom-in nearshore views (pink dashed box) of current velocities plotted on vorticity (ω) colormaps, with identified flash rips numbered in circles.

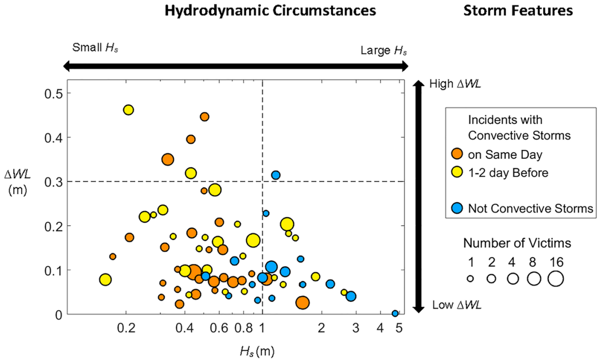

Fig 7. Distribution of drowning incident events (based on GLCID data) plotted in terms of the meteorologically induced water level changes ΔWL versus the significant wave height of wind waves H_s (in log scale). The size of dots is proportional to the number of victims in each incident. Orange dots represent incidents associated with convective storms on the same day; yellow dots represent those associated with convective storms crossing over the lake 1-2 days before; and blue dots represent those associated with not convective types of storms.

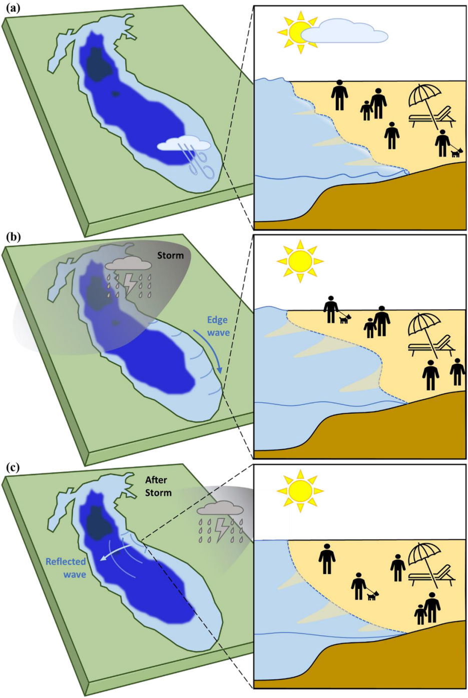

Fig 8. Three conditions of hidden flash rips at the beach (depicted as sediment plumes): (a) A series of small convective cluster storms; mild nearshore wave breaking in a fair weather condition; (b) A convective storm passing somewhere of the lake but far away from the beach; the meteotsunami-generated edge waves propagating to the beach with relatively clam water hours later in a dry weather condition; (c) After a passing storm, unnoticeable reflected meteotsunami waves to the beach with tranquil water in a dry weather condition..

Table 1. Summary of convective storms with atmospheric disturbances, meteotsunamis and wave conditions, and related drowning incidents.

Convective storms					Atmospheric Disturbances[c]				Meteotsunamis[d]				Waves[e]			Incidents[f]				
#S	Time (UTC)	Type[a]	Speed (m/s)	Dir[b]	max ΔP/10min (hPa)	W_{max} (m/s)	%P	%W	Time (UTC)	NOS Gage	max ΔWL (m)	T (min)	H_s (m)	T_p (sec)	MWD	Time (UTC)	Location	#I	F	R
S1	0718 1125 -1855	C	14.6	127	2.3	15.4	58	42	0718 1857-2357	CAL	0.36	48	1.28	5.5	247	0719 0000	Ludington	I1	1	0
S2	0719 0755-1355	CL	22.8	119	1.9	12.3	28	72	0719 1457-1703	CAL	0.31	118	0.6	4.2	280	0719 1630-1700	South Haven	I2	0	3
													0.13	1.6	92	0719 2300	Kenosha	I3	1	0
S3	0720 0225-0955	B	16.5	179	3.7	15.9	40	60	-	-	-	-								
S4	0720 1655 -2325	L	20.7	162	6.9	18.0	41	59	0720 1809 -0721 0957	LUD	0.32	72	0.75	4.8	4	0721 0130	Michigan City	I4	1	0
									0720 1903 -0721 0145	MKE	0.35	39								
									0720 2336 -0721 0151	CAL	0.77	99								
S5	0721 0455-1325	CL	9.8	108	0.9	7.2	64	36	0721 1003-1157	CAL	0.55	114	0.44	2.8	307	0721 1600-1900	Ludington	I5	0	1
S6	0721 1625 -2255	C	7.0	82	0.3	10.3	23	77	-	-	-	-	0.93	3.7	33	0721 2030	Chicago	I6	1	1

[a] C: Complex, CL: Cluster, B: Bow, L: Linear
[b] Dir: storm propagation direction
[c] ΔP: pressure change, W_{max}: max wind speed, %P (%W): relative contribution of atmospheric pressure (wind stress) to initiate water level fluctuations
[d] ΔWL: height from crest to trough; T: period, H_s: significant wave height, T_p: peak wave period, MWD: mean wave direction
[f] F:number of drowning fatalities, R: number of rescues

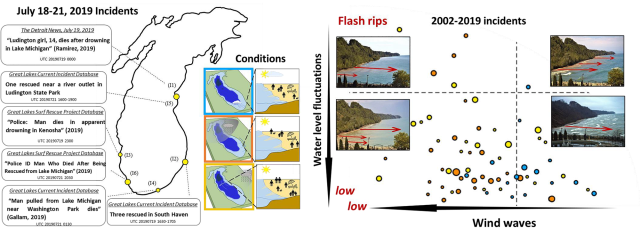
July 18-21, 2019 Incidents
The Detroit News, July 19, 2019
"Ludington girl, 14, dies after drowning in Lake Michigan" (Ramirez, 2019)
UTC 20190719 0000
Great Lakes Current Incident Database
One rescued near a river outlet in Ludington State Park
UTC 20190721 1600-1900
Great Lakes Surf Rescue Project Database
"Police: Man dies in apparent drowning in Kenosha" (2019)
UTC 20190719 2300
Great Lakes Surf Rescue Project Database
"Police ID Man Who Died After Being Rescued from Lake Michigan" (2019)
UTC 20190721 2030
Great Lakes Current Incident Database
"Man pulled from Lake Michigan near Washington Park dies" (Gallam, 2019)
UTC 20190721 0130
Great Lakes Current Incident Database
Three rescued in South Haven
UTC 20190719 1630-1705
(I1)
(I5)
(I3)
(I6)
(I4)
(I2)
Conditions
Flash rips
2002-2019 incidents
Water level fluctuations
low
low
Wind waves